Geophysical Research Letters

RESEARCH LETTER
10.1029/2025GL114987

Contributions of Atmospheric Ridging and Low Soil Moisture to the Record-Breaking June 2023 Mexico-Texas Heatwave

Dmitri A. Kalashnikov[1,2], Deepti Singh[1], Mingfang Ting[3,4], and Benjamin I. Cook[3,5]

[1]School of the Environment, Washington State University, Vancouver, WA, USA, [2]Sierra Nevada Research Institute, University of California Merced, Merced, CA, USA, [3]Lamont-Doherty Earth Observatory, Columbia University, New York, NY, USA, [4]Columbia Climate School, Columbia University, New York, NY, USA, [5]NASA Goddard Institute for Space Studies, New York, NY, USA

Abstract June 2023 witnessed the hottest, largest, and longest-lasting heatwave across Mexico and Texas between 1940 and 2023. We apply constructed analogs with multiple linear regression models to quantify the contribution of different drivers to daily temperature anomalies during this heatwave. On the hottest day (20 June), circulation, soil moisture, and their interaction explained 3.82°C (90% CI: 2.72–4.91°C) of the 5.42°C observed anomaly with most of the residual attributed to the thermodynamic effects of long-term warming. Using CESM2-LENS2, we find that June 2023-like patterns are not projected to increase in frequency but will become 1.9°C hotter by the mid-21st century under SSP3-7.0. The hottest simulated day with these patterns could produce temperatures >50°C (122°F) across south Texas, representing a low-likelihood yet physically plausible worst-case scenario that could inform disaster preparedness and adaptation planning.

Plain Language Summary During summer 2023, multiple heat waves affected Mexico and Texas and contributed to hundreds of heat-related fatalities and thousands of heat-related emergency-room visits. Particularly notable was an unusually intense and persistent early-season heat wave in June, when numerous locations exceeded their all-time record highs. This heatwave was the hottest, largest, and longest-lasting heatwave to affect the Mexico-Texas region in the observational record spanning 1940–2023. In this study, we quantify the influence of atmospheric circulation and soil moisture on the heatwave intensity. We find that these factors together account for most of the extreme temperature anomaly at the peak of the heatwave, with most of the remainder explained by long-term warming. We also find that June 2023-like circulation patterns will not occur more frequently but are projected to become nearly 2°C hotter than present by the mid-21st century. The hottest simulated day with these patterns could produce widespread temperatures hotter than 50°C (122°F) across south Texas. Although these temperatures have a low probability of occurrence, they represent physically plausible conditions that could threaten human survivability. Such low-likelihood, yet high-risk scenarios can inform disaster preparedness and adaptation planning efforts.

Dmitri A. Kalashnikov and Deepti Singh contributed equally to this work.

Key Points:

- A heatwave with record-breaking intensity, persistence, and spatial extent affected Mexico and Texas during June 2023
- Circulation, record-low soil moisture, and their interaction explain most of the temperature anomaly at peak of heatwave
- June 2023-like patterns are projected to warm an additional 1.9°C by the mid-21st century due to regional warming and drying

Supporting Information:

Supporting Information may be found in the online version of this article.

Correspondence to:

D. A. Kalashnikov and D. Singh,
dkalashnikov@ucmerced.edu;
deepti.singh@wsu.edu

Citation:

Kalashnikov, D. A., Singh, D., Ting, M., & Cook, B. I. (2025). Contributions of atmospheric ridging and low soil moisture to the record-breaking June 2023 Mexico-Texas heatwave. *Geophysical Research Letters*, *52*, e2025GL114987. https://doi.org/10.1029/2025GL114987

Received 23 JAN 2025
Accepted 14 FEB 2025

Author Contributions:

Conceptualization: Dmitri A. Kalashnikov, Deepti Singh, Mingfang Ting, Benjamin I. Cook
Data curation: Dmitri A. Kalashnikov
Formal analysis: Dmitri A. Kalashnikov
Funding acquisition: Dmitri A. Kalashnikov, Deepti Singh
Investigation: Dmitri A. Kalashnikov
Methodology: Dmitri A. Kalashnikov, Deepti Singh, Mingfang Ting, Benjamin I. Cook
Project administration: Deepti Singh
Resources: Deepti Singh

1. Introduction

Across Mexico and Texas (hereafter, "MXTX"), a prolonged heatwave during June 2023 severely impacted the region's population and infrastructure. Several cities broke all-time records on multiple days, including San Angelo, Texas (45.6°C on the 20th–21st) and Chihuahua, Mexico (42.0°C on the 22nd and 24th) (National Weather Service, 2023; Stillman et al., 2023). Persistent high temperatures contributed to >100 human deaths, >1000 heat-related emergency room visits, and numerous cattle deaths in Mexico (Cantú, 2023; Deutsche Welle, 2023), and >11 deaths with a surge in heat-related emergency room visits in Texas (Douglas, 2023; Pskowski & Gina, 2023).

The June 2023 MXTX heatwave (hereafter, "MXTX2023") was associated with a strong subtropical ridge. Ridges provide the synoptic forcing for heatwaves by limiting moisture transport to the region, suppressing convection and increasing incoming surface solar radiation due to reduced cloud cover. Further, low soil moisture (SM) can amplify heatwaves via changes in surface energy partitioning and land-atmosphere feedbacks (Koster et al., 2006; Miralles et al., 2019; Wehrli et al., 2019). MXTX is a hotspot of land-atmosphere coupling (Benson & Dirmeyer, 2021; Miralles et al., 2012; Zscheischler & Seneviratne, 2017). Indeed, studies of previous major heatwaves such as in the 1930s (Meehl et al., 2022), 1998 (Hong & Kalnay, 2000) and 2011 (Hoerling et al., 2013; Seager

Software: Dmitri A. Kalashnikov
Supervision: Deepti Singh
Validation: Dmitri A. Kalashnikov
Visualization: Dmitri A. Kalashnikov
Writing – original draft: Deepti Singh
Writing – review & editing: Dmitri A. Kalashnikov, Mingfang Ting, Benjamin I. Cook

et al., 2014) found evidence of drought-driven amplification of heat extremes. SM interactions also increased the intensity of numerous recent heatwaves globally, in some cases being the primary driver of record heat rather than large-scale circulation patterns (Wehrli et al., 2019).

Extreme event attribution studies have linked the increased likelihood and severity of heatwaves across most regions including MXTX to anthropogenic warming (National Academies of Sciences, Engineering, and Medicine, 2016; Otto, 2023; Seneviratne et al., 2021; Swain et al., 2020). For example, Hoerling et al. (2013) found that anthropogenic warming accounted for approximately 20% of the magnitude of the 2011 extreme Texas heat and Rupp et al. (2015) found that anthropogenic warming made those temperatures ∼10 times more likely. More recently, Trok et al. (2024) found an anthropogenic contribution of 1.18–1.42°C to the MXTX2023 heatwave. A subset of attribution studies that conduct such analyses conditioned on the atmospheric circulation are referred to as the circulation-analogs or dynamical-adjustment approach (Faranda et al., 2022; Terray, 2021; Yiou et al., 2017). These studies enable the quantification of the relative influence of different physical drivers and have been applied to quantify the influence of circulation and other factors on heatwaves in Europe (Jézéquel et al., 2018; Lemus-Canovas et al., 2024; Yiou et al., 2007), Argentina (Collazo et al., 2024), and China (Huang et al., 2024).

We apply this circulation-analogs approach to investigate the contribution of different drivers to the MXTX2023 heatwave. Specifically, we address three questions: (a) How unique was the extent, intensity, and persistence of this heatwave in the long-term record? (b) What was the relative influence of atmospheric circulation and SM on heatwave intensity? (c) Are the key drivers of the MXTX2023 heatwave projected to change with continued warming? Understanding changes in the drivers of heatwaves is important for accurately predicting and projecting their risk, and informing heat preparedness efforts (Domeisen et al., 2023).

2. Materials and Methods

2.1. Data

We use daily-maximum 2-m temperature (T_{max}), daily-average 500-hPa geopotential heights (Z_{500}) and daily-average near-surface SM derived from the European Center for Medium-Range Weather Forecasts ERA5 reanalysis at 0.25° resolution (Hersbach et al., 2023). We use ERA5 based on its superior performance in simulating subseasonal-to-seasonal variations and long-term trends in SM in recent decades relative to other reanalysis products when compared with in-situ observations (Li et al., 2020), its strong correlation with satellite-derived estimates (Lal et al., 2022), and the availability of high-resolution, long-term data over the analysis period. Standardized T_{max} anomalies are obtained by first calculating area-weighted, domain-averaged T_{max} across the full extent of MXTX. Then, the climatological mean and standard deviation of daily 1991–2020 T_{max} is computed from 15-day moving windows. Daily anomalies are then calculated by removing this climatological daily mean and dividing by the standard deviation. We also analyze these variables from the NCAR Community Earth System Model Large Ensemble (CESM2-LENS2; hereafter "CESM2") at 0.94° × 1.25° spatial resolution using the SSP3-7.0 scenario (Rodgers et al., 2021). Of the 100 available CESM2 ensemble members, 50 use prescribed CMIP6 biomass burning emissions, and the rest use smoothed emissions. For consistency, we analyze the 40 members with CMIP6 biomass burning emissions that include SM.

2.2. Constructed Analogs

We use constructed analogs, a modification of the widely-used flow-analogs approach (Faranda et al., 2022; Jézéquel et al., 2018; Yiou et al., 2007, 2017), to quantify the contributions of circulation and SM to daily T_{max} anomalies during the MXTX2023 heatwave. This methodology estimates the magnitude of surface variables such as temperature during extreme events from a set of circulation analogs identified over a specific historical period. A linear regression model is trained from historical analog patterns to predict an associated variable from the target pattern in the present climate (Tippett & DelSole, 2013). This method has been recently used to diagnose vapor pressure deficit trends over the western U.S. (Zhuang et al., 2021) and the drivers of the 2022 Yangtze River Basin heatwave (Huang et al., 2024). We modify this approach to incorporate SM in the linear model to develop the constructed analogs.

Our method uses standardized, detrended Z_{500} anomalies as a measure of circulation to construct analogs, following Jézéquel et al. (2018) and Zhuang et al. (2021). As with T_{max}, Z_{500} is deseasonalized and standardized

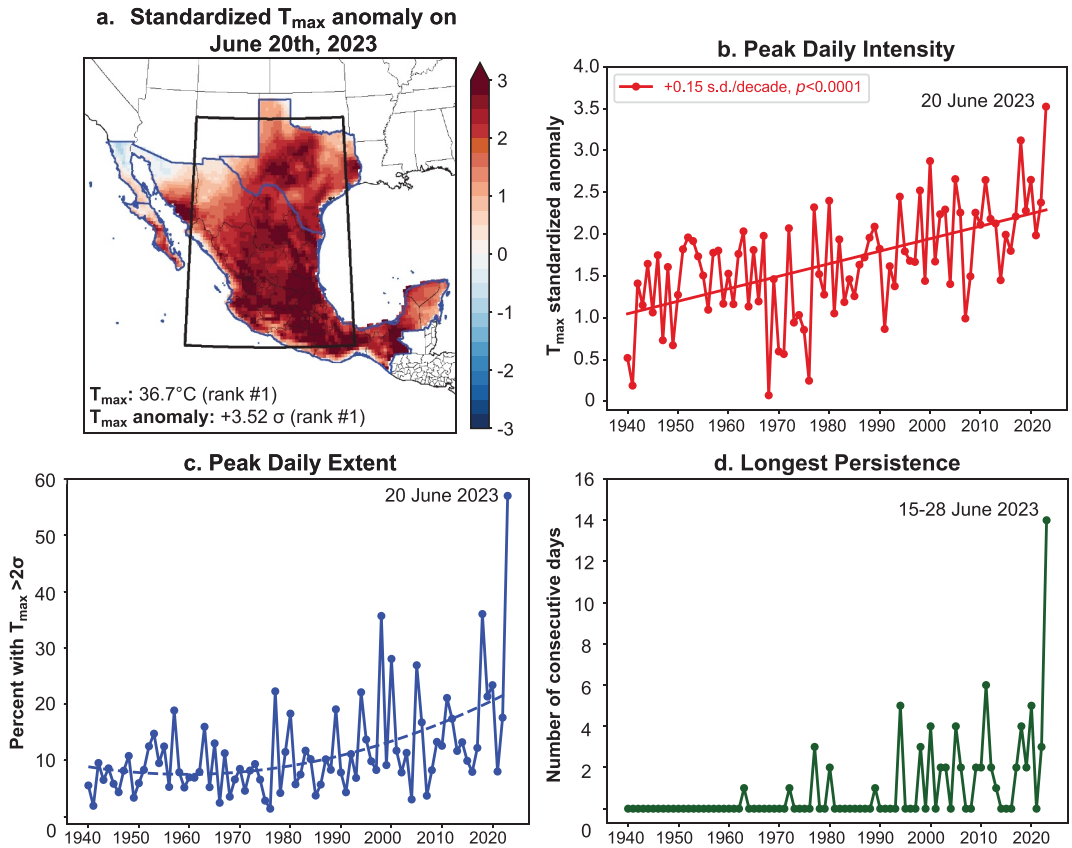

Figure 1. (a) Standardized T_{max} anomalies on 20 June 2023. Daily anomalies are calculated relative to the April–September climatology (1991–2020). Time series (1940–2023) of the highest (b) daily intensity: area-averaged T_{max} anomalies, (c) fraction of the domain experiencing $T_{max} > 2\sigma$, and (d) most consecutive days with area-average $T_{max} > 2\sigma$. Black rectangle in panel (a) shows the domain for pattern-matching to identify analogs.

by subtracting the 1991–2020 climatological means computed in 15-day moving windows, and dividing by the standard deviation in each window. We use Pearson's correlation to identify spatially similar circulation analogs over a bounding box encompassing central/northern Mexico and Texas (17–35°N; 109–95°W; Figure 1a). To remove the effect of thermal expansion, Z_{500} is detrended prior to analog matching by subtracting the average hemisphere-mean Z_{500} change between latitude 17–35°N at each year since 1940. This approach provides an advantage over linear detrending as global Z_{500} changes have not been linear over the period of record owing to the pause in warming between the 1950–1970s. For each day in 2023, we extract the 100 closest analogs from historical (1940–2022) warm-season (April–September) days within a 61-day window centered on that day. We tested 20–100 analogs and although higher analog counts slightly reduce median correlation with the target pattern, we chose 100 analogs to increase sample size (Figure S1 in Supporting Information S1). To enforce analog independence, we select only one best-matching pattern from centered 7-day windows.

Using the 100-closest analogs, a constructed analog is created for each day of the heatwave to predict the domain-averaged, detrended (denoted with $'$) T_{max} ($\hat{T}'_{max}$) using linear regression. $\hat{T}'_{max}$ is computed from the combined MXTX domain and is detrended by subtracting the annual ERA5 global-mean temperature change at each year since 1940 (T_{trend}). We first develop two linear regression models from the historical analogs - simple linear regression with detrended, domain-maximum Z_{500} (Z'_{500max}) from the analog day as the predictor:

$$\hat{T}'_{max} = \beta_0 + \beta_1 Z'_{500max} \quad (1)$$

and a multiple linear regression model with same-day Z'_{500max} and domain-averaged SM anomalies from the prior day (SM_{lag1}) as predictors:

$$\hat{T}'_{max} = \beta_0 + \beta_1 Z'_{500max} + \beta_2 SM_{lag1} \quad (2)$$

Note that SM is not detrended due to lack of a significant long-term trend since 1940 (Figure S2 in Supporting Information S1). Due to the strong coupling between T_{max} and SM over this region (e.g., Miralles et al., 2012), these variables show significant ($p < 0.01$) bi-directional Granger causality at all lags between 1 and 7 days (Figure S3 in Supporting Information S1). To control for endogeneity, we use SM_{lag1} rather than same-day SM to predict $\hat{T}'_{max}$. The first model estimates the contribution of circulation alone while the second model estimates the combined contribution of circulation and antecedent SM to observed daily T_{max}. We then train a third model that includes a same-day Z_{500}*SM interaction term to help explain the residual from the second model, as nonlinear amplifying effects of dry SM on T_{max} are expected under strong ridging:

$$\hat{T}'_{max} = \beta_0 + \beta_1 Z'_{500max} + \beta_2 SM_{lag1} + \beta_3 Z'_{500max} \cdot SM \quad (3)$$

As a final step, we add T_{trend} to output from the third model to account for long-term warming. For all models, 90% confidence intervals (CI) of the predictions are derived from the standard errors of the regression coefficients. $\hat{T}'_{max}$ values are converted to anomalies relative to 1991–2020 for presentation of results.

2.3. Projections of MXTX2023-Like Patterns and Associated T_{max}

Using Pearson's correlation, we identify days in the 40 CESM2 ensemble members with Z_{500} patterns similar (correlation >0.8) to the observed pattern on 20 June 2023. Then, we analyze simulated T_{max} on those days during historical (2000–2020) and mid-century (2040–2060) periods. For this step, Z_{500} from ERA5 is regridded to the native resolution of CESM2 using bilinear interpolation to ensure consistent analog matching between reanalysis and model output. We remove the effect of thermal expansion on Z_{500} in CESM2 by subtracting the ensemble-mean Z_{500} change from each year since 1940. To test whether drier soils will significantly influence T_{max} on pattern-days in the future, we compare T_{max} anomalies under both dry and wet SM conditions defined using the 33rd and 66th percentiles.

3. Results and Discussion

3.1. The Record-Breaking MXTX2023 Heatwave

The MXTX2023 heatwave had record-breaking intensity, spatial extent, and persistence (Figure 1). The heatwave peaked on 20 June 2023 with a domain-average T_{max} of 36.7°C and anomaly of +5.42°C (+3.52σ), the hottest among all historical warm-season days (Figures 1a and 1b). 57% (1.49 million km^2) of the region experienced local T_{max} anomalies exceeding 2σ on 20 June, which is ∼1.6 times higher than the previous largest extent observed on 23 July 2018 (943,000 km^2; Figure 1c). Domain-average T_{max} anomalies >2σ persisted for 14 consecutive days (15–28 June), more than double the previous longest heatwave persistence of 6 days in 2011 (Figure 1d). The extreme and long-lasting heat over this region during summer 2023, including additional heatwaves in the following months, have been attributed to atmospheric blocking forced by record-warm north Atlantic sea surface temperatures and the developing El Niño event at that time (Lopez et al., 2024).

The characteristics of the MXTX2023 heatwave are also aligned with their long-term trajectories (Figures 1b–1d). Peak daily T_{max} anomalies have increased linearly at ∼0.15σ/decade, representing a doubling since 1940. The regional extent and persistence of extreme heat has increased non-linearly over this period: 18 of the recent 30 years had at least one day with domain-average $T_{max} > 2\sigma$, while only 5 years between 1940 and 1990 experienced such widespread T_{max} anomalies. These trends are consistent with previous studies that also found increases in various measures of frequency, intensity and extent of heatwaves across Mexico and the southern U.S (García-Cueto et al., 2020; Keellings & Moradkhani, 2020; Marvel et al., 2023; Murray-Tortarolo, 2021; Perkins-Kirkpatrick & Lewis, 2020; Singh et al., 2024).

3.2. Temporal Evolution of Z_{500}, T_{max}, and SM

Figure 2a shows the temporal evolution of domain-averaged T_{max}, Z_{500}, and SM anomalies during June 2023. Between 15 and 28 June, T_{max} anomalies consistently exceeded +2σ and nearly every day exceeded their daily record (Figure 2a). These temperatures were accompanied by positive Z_{500} anomalies, though their magnitude

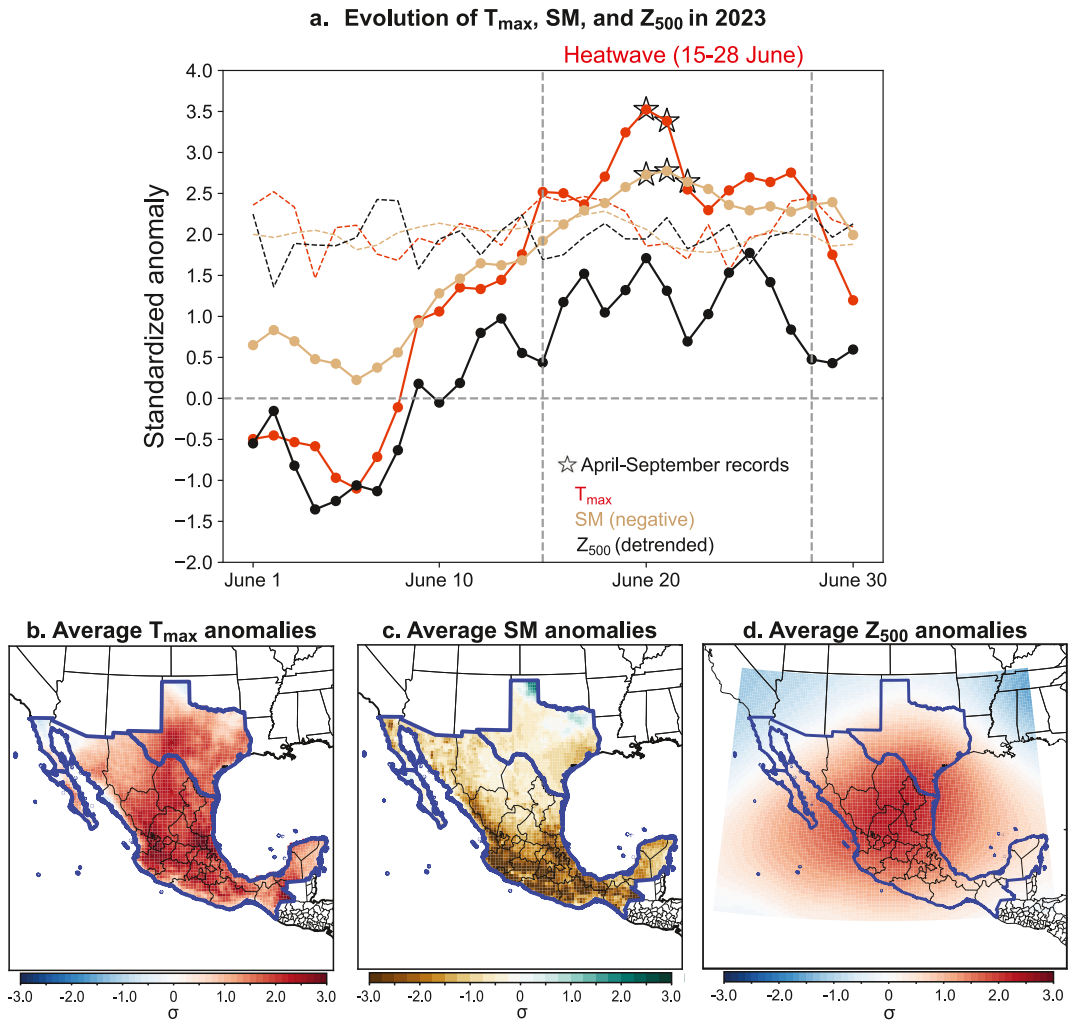

Figure 2. (a) Temporal evolution of T_{max} (red), negative soil moisture (SM, brown), and detrended Z_{500} (black) anomalies during June 2023. Note: SM is inverted—positive values indicate drier conditions. Dashed lines indicate historical daily records (1940–2022). Stars indicate occurrence of record highest warm-season values among all days during 1940–2023. Average anomalies of (b) T_{max}, (c) SM, and (d) detrended Z_{500} over 15–28 June.

was not exceptional relative to the background atmospheric flow for most of the event. This suggests that the circulation contributed to the development of the heatwave but the extreme temperatures were driven by additional factors such as dryness. SM conditions were relatively dry from early June and the dryness strengthened simultaneously with increasing T_{max} and Z_{500} anomalies (Figure 2a). Negative SM anomalies exceeded 2σ on 16 June and were consistently at record-low daily values between 17 and 30 June. Further, SM on the two days that exceeded the historically hottest warm-season temperatures (20–21 June) was also historically lowest.

Average T_{max} anomalies during the heatwave (15–28 June) were positive across the domain and exceeded $+2\sigma$ across western Texas and central Mexico (Figure 2b). The largest negative SM anomalies were in central and southern Mexico, slightly south of the peak Z_{500} anomalies associated with the subtropical ridge (Figures 2c and 2d). The ridge amplified on 20 June, coincident with peak T_{max} anomalies, then weakened and shifted northward and subsequently re-strengthened on 25 June (Figure S4 in Supporting Information S1). This atmospheric circulation pattern persisted for 10 consecutive days (12–21 June), which is unprecedented in the historical record (Figure S5 in Supporting Information S1). This suggests that the unusually persistent ridge triggered the heatwave, contributed to its exceptional persistence, and likely exacerbated the already dry SM conditions. Likewise, the close coevolution of positive T_{max} and negative SM anomalies, including their record strength and concurrence of their peaks, is not surprising given the strong temperature-SM coupling over this region and suggests that

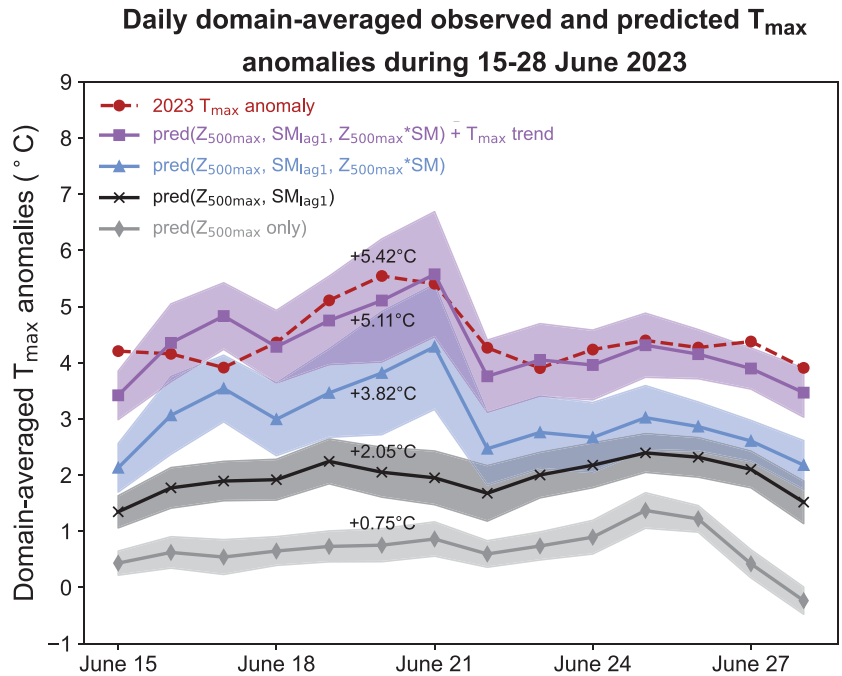

Figure 3. Observed (red) and predicted daily domain-averaged T_{max} anomalies from constructed analogs using Z'_{500max} (light gray), Z'_{500max} and SM_{lag1} (black), Z'_{500max}, SM_{lag1}, and $Z'_{500max} \cdot SM$ interaction term (blue), and Z'_{500max}, SM_{lag1}, $Z'_{500max} \cdot SM$ interaction term, and long-term warming (purple). Constructed analogs are created for each day individually. Shading represents the 90th percentile confidence intervals around these estimates. Text shows values for 20 June. See Figure S7 in Supporting Information S1 for T_{max} actual values.

land-atmosphere feedbacks acted to amplify the heatwave intensity (Benson & Dirmeyer, 2021; Wehrli et al., 2019).

3.3. Disentangling Heatwave Drivers Using Constructed Analogs

Constructed analogs based solely on Z'_{500max} predict $\hat{T}'_{max}$ anomalies between 3.0 and 4.8°C cooler than observed T_{max} on MXTX2023 days (Figure 3, gray line), indicating a substantial role of factors beyond circulation. Including SM_{lag1} adds 0.9–1.8°C to $\hat{T}'_{max}$ (Figure 3, black line), while the $Z'_{500max} \cdot$ SM interaction term adds a further 0.5–2.3°C (Figure 3, blue line). The predicted $\hat{T}'_{max}$ anomaly for 20 June, the peak of the heatwave, is +0.75°C from Z'_{500max} alone (90% CI: 0.46–1.05°C), +2.05°C from Z'_{500max} and SM_{lag1} (90% CI: 1.61°C–2.49°C), and +3.82°C when including the $Z'_{500max} \cdot$ SM interaction term (90% CI: 2.72–4.91°C). The interaction term therefore explains 1.77°C (~33%) of the observed +5.42°C T_{max} anomaly on 20 June, reflecting the substantial amplifying influence of ridging-SM interaction on heat extremes in this region. The three factors together explain 3.82°C (~70%) of the observed T_{max} anomaly. These results are largely stable when using 60–100 analogs for daily pattern matching (Figure S6 in Supporting Information S1). Adding the T_{trend} (+1.29°C) to account for part of the thermodynamic residual yields a predicted $\hat{T}'_{max}$ anomaly of +5.11°C on 20 June, with the observed anomaly falling within the 90% CI of this prediction (4.01–6.20°C).

Notably, the dynamic contribution obtained from the Z'_{500max}-only analogs is much smaller than the dynamic contribution recently attributed to mid-latitude heatwaves (e.g., Terray, 2021, 2023). The dynamic contribution of 0.75°C on 20 June represents ~14% of the observed T_{max} anomaly, and suggests a more pronounced role of SM and circulation-SM interactions in this largely semi-arid region at the tropical-subtropical margin. Indeed, the combined contribution of SM_{lag1} and $Z'_{500max} \cdot$ SM of 3.07°C represents ~57% of the total T_{max} anomaly on 20 June. This is in contrast to some recent studies (e.g., Bercos-Hickey et al., 2022; Conrick & Mass, 2023) that found only a limited role of SM in amplifying a major mid-latitude heatwave where dynamics play a larger role. However, our results agree with Wehrli et al. (2019), who reported a larger contribution of SM than circulation for a comparable subtropical heatwave in southern Africa during austral summer 2015–2016.

Meanwhile, the +1.29°C T_{trend} from ERA5 is consistent with the 1.18–1.42°C anthropogenic contribution directly attributed to this heatwave by Trok et al. (2024). Similar anthropogenic contributions have been attributed to other heatwaves using varying methodologies, including ∼1.0–1.2°C for the 2010 Russian heatwave (Terray, 2021; Wehrli et al., 2019) and ∼0.8–2.0°C for the June 2021 western North American heatwave (Bercos-Hickey et al., 2022; Philip et al., 2022; Terray, 2023). Our approach of using a fixed anthropogenic contribution allows us to estimate a residual that is not accounted for by any of the physical drivers, including long-term warming. For example, 0.31°C of the T_{max} anomaly on 20 June remains unexplained by our analogs. This could be because extreme heatwaves such as MXTX2023 understandably do not have good historical analogs (van den Dool, 1994; van Oldenborgh et al., 2022). Our approach also does not capture the effects of unprecedented spatial extent and persistence of heat during the MXTX2023 heatwave (Miralles et al., 2019; Neal et al., 2022; Qiao et al., 2023). Additionally, land cover changes (i.e., deforestation and urbanization) in Mexico have the potential to further exacerbate present-day T_{max} compared to historical analogs (Englehart & Douglas, 2005; Stahle et al., 2009).

3.4. Historical and Projected Changes in June 2023-Like Circulation Patterns

Circulation patterns similar to 20 June 2023 (correlation >0.8, hereafter "2023-like") have decreased in frequency by ∼2 days since 1940, and this trend is supported by a decrease in the CESM2 ensemble mean of ∼1.8 days (Figure 4a). However, domain-averaged T_{max} on days with these circulation patterns has increased significantly (+1.9°C) since 1940 and has outpaced the CESM2 ensemble mean increase of +1.2°C (Figure 4b). SM shows a weak increasing trend in observations (Figure 4c), but this is largely due to persistent drought in the early part of the record that peaked in the 1950s (Stahle et al., 2009). Over recent decades, SM has been declining and this negative trend is also present in CESM2 (Figure 4c, Figure S2 in Supporting Information S1). The observed frequency of the circulation patterns and corresponding T_{max} and SM fall within the CESM2 ensemble spread (Figures 4a–4c). CESM2 also simulates a similar dependence of T_{max} on Z_{500} and SM (Figure S8 in Supporting Information S1), making it a suitable model for this analysis.

Leveraging the CESM2 ensemble spread, we investigate changes in T_{max} and SM associated with 2023-like patterns between the historical (2000–2020) and mid-21st century (2040–2060) periods. The sample size in each period is 840 years (21 years × 40 members). The median frequency of 2023-like patterns does not change between the historical period and mid-century, remaining at five days per warm season (Figure 4d). However, median T_{max} during 2023-like patterns increases steadily with warming, at a faster rate than the seasonal-mean warming. Median domain-average T_{max} is projected to be 1.9°C higher by mid-21st century, increasing from 31.7 to 33.6°C (Figures 4e, 4g, and 4h; Figure S9 in Supporting Information S1) while the seasonal-mean T_{max} is projected to warm by 1.4°C (not shown) (Note that these results are based on T_{max} directly simulated by CESM2 on days with 2023-like patterns, rather than predictions from the constructed analog models). These circulation patterns are projected to occur with drier conditions—median SM anomalies are -0.60σ by mid-century compared to -0.37σ during historical (Figure 4f). Further, median T_{max} is ∼0.4°C hotter when 2023-like patterns coincide with dry relative to wet SM conditions and the upper range of possible temperatures is also substantially higher (Figure S10 in Supporting Information S1).

Using other correlation thresholds between 0.7 and 0.9 for pattern matching in CESM2 produces similar long-term changes in pattern frequency (decrease of 0–1 day), T_{max} (1.8–2.1°C increase), and SM (0.21–0.30σ decrease) (Figure S11 in Supporting Information S1). The hottest simulated day with 2023-like patterns by mid-century has domain-average T_{max} of 40.4°C with south Texas above 50°C (122°F; Figure 4i). Such temperatures would exceed the current Texas record maximum of 48.9°C (120°F; National Centers for Environmental Information, 2024) over large areas and pose an acute risk to human life, non-human species, and agriculture in the absence of sufficient adaptation.

4. Conclusions

The record-breaking MXTX2023 heatwave was the hottest, largest, and longest-lasting across this region over 1940–2023. At the peak of the heatwave (20 June), constructed analogs based solely on Z'_{500max} predict a domain-averaged T_{max} anomaly of only +0.75°C. However, the combined contributions of circulation, low SM, and their interaction explain 3.82°C (∼70%) of the observed anomaly of +5.42°C on 20 June, with most of the residual contributed by long-term warming since 1940. Our results emphasize that circulation dynamics alone are

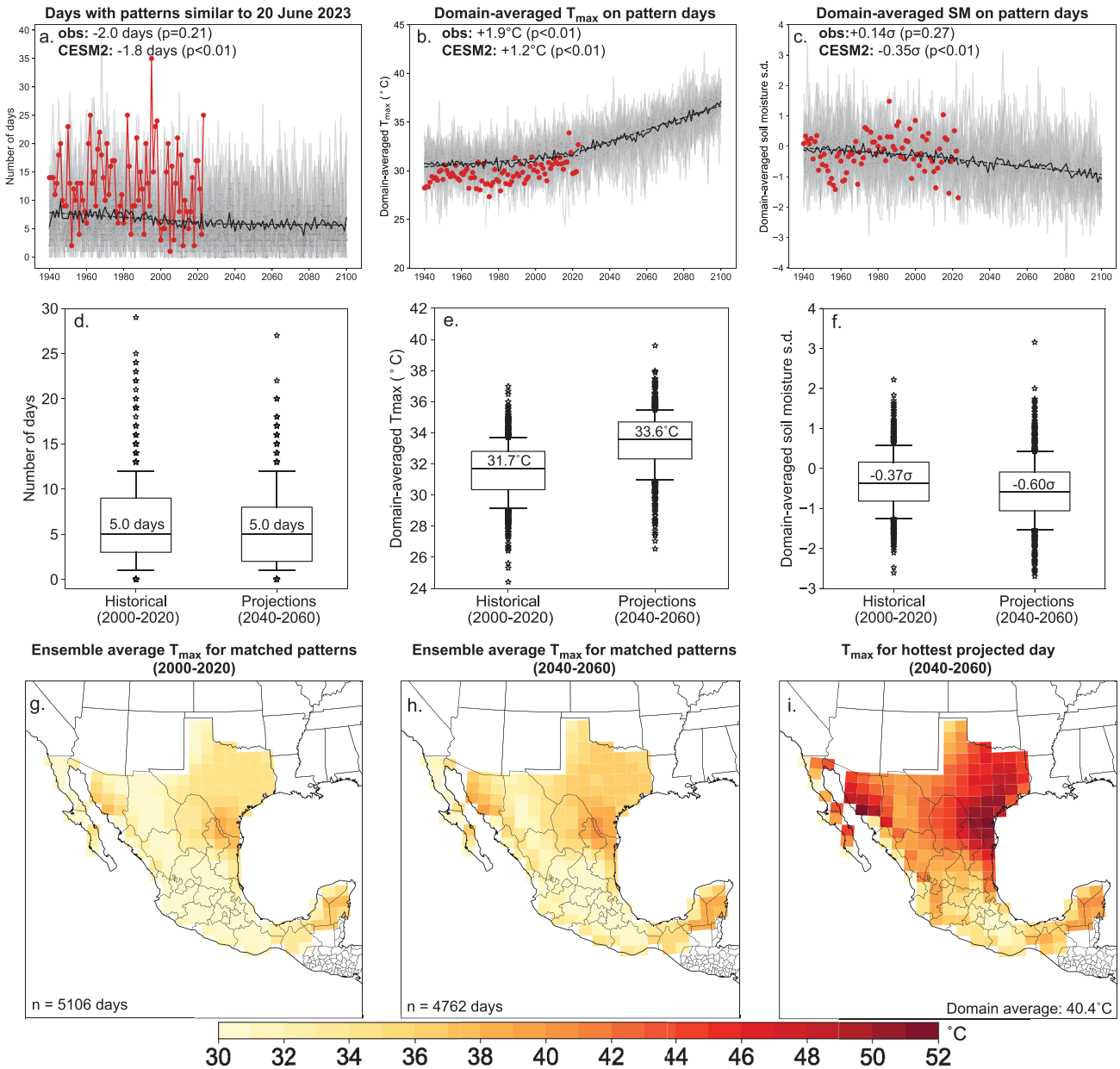

Figure 4. Time series of (a) days in each season (April–September) with 20 June 2023-like patterns, and domain-average (b) T_{max} and (c) SM on those days. Black lines represent CESM2 ensemble means, gray lines represent each ensemble member and red represents observations from ERA5. Inset text in panels (a)–(c) shows observed and CESM2-simulated changes over 1940–2023 and *p*-values obtained from a permutation test. (d)–(f) Distributions of seasonal averages of each variable in historical (2000–2020) and future (2040–2060) on all matched pattern days in the CESM2 ensemble. Text in boxplots indicates median values. (g)–(h) Average T_{max} on historical and future days with 20 June-like patterns. (i) T_{max} on the hottest simulated day in the mid-21st century. Text in (g)–(h) shows the number of simulated 2023-like patterns across 840 model-years (21 years × 40 ensemble members).

insufficient to explain the magnitude of the MXTX2023 heatwave, and that amplifying effects of dry SM must be considered when assessing heatwaves over this region. Further, our findings suggest that future extreme heatwaves over MXTX will show less dependence on rare circulation anomalies under projected warming and drying. Recent studies using constructed analogs have also failed to explain anomalies solely through circulation, leaving a large residual attributed to other factors such as thermodynamic effects of anthropogenic warming (Huang et al., 2024; Zhuang et al., 2021). Our study extends the constructed analogs approach to directly incorporate SM, and our methodology can be applied to other heatwaves globally.

Using CESM2, we show that June 2023-like circulation patterns will warm an additional 1.9°C by mid-century, and the hottest day could produce widespread T_{max} >50°C (122°F) across south Texas. This represents a low-likelihood yet physically plausible worst-case scenario that can inform disaster preparedness and adaptation planning. We note that this result is based on one climate model with a relatively high climate sensitivity, so we largely limit our analysis to the mid-century when global temperature projections of ∼1.7–2.5°C above pre-industrial do not diverge substantially from other climate models (Gettelman et al., 2019; Meehl et al., 2020). We selected CESM2 as large ensembles offer the ability to evaluate a range of outcomes due to natural variability, and a larger sample size for understanding the drivers of rare events (Deser et al., 2012; Lehner & Deser, 2023; McKinnon & Simpson, 2022). Combined with observation-based constructed analogs, this approach can be leveraged to assess the drivers and risk of rare, high-impact events such as the MXTX2023 heatwave in a changing climate.

Data Availability Statement

ERA5 data can be accessed at Hersbach et al. (2023). CESM2-LENS2 data can be accessed at Community Earth System Model (2024). Derived data sets used to perform analyses are available at Kalashnikov (2025a). Analysis code can be accessed at Kalashnikov (2025b).

Acknowledgments
This research used resources from the Center for Institutional Research Computing at Washington State University. Support for DAK was provided by NSF AGS-PRF #2403765, DS by NSF AGS #2206996, and BIC by NASA's Modeling, Analysis, and Prediction program. Additional support for DAK and DS was provided by NASA FINESST award 80NSSC21K1603.

References

Benson, D. O., & Dirmeyer, P. A. (2021). Characterizing the relationship between temperature and soil moisture extremes and their role in the exacerbation of heat waves over the contiguous United States. *Journal of Climate*, *34*(6), 2175–2187. https://doi.org/10.1175/JCLI-D-20-0440.1

Bercos-Hickey, E., O'Brien, T. A., Wehner, M. F., Zhang, L., Patricola, C. M., Huang, H., & Risser, M. D. (2022). Anthropogenic contributions to the 2021 Pacific Northwest heatwave. *Geophysical Research Letters*, *49*(23), e2022GL099396. https://doi.org/10.1029/2022GL099396

Cantú, E. (2023). Heat Wave in Mexico: Hermosillo Above 120 Degrees. Retrieved from https://www.nytimes.com/2023/07/06/world/americas/hermosillo-mexico-heat.html

Collazo, S., Suli, S., Zaninelli, P. G., García-Herrera, R., Barriopedro, D., & Garrido-Perez, J. M. (2024). Influence of large-scale circulation and local feedbacks on extreme summer heat in Argentina in 2022/23. *Communications Earth & Environment*, *5*(1), 1–17. https://doi.org/10.1038/s43247-024-01386-8

Community Earth System Model (CESM). (2024). Data sets available to the community [Dataset]. *Community Earth System Model (CESM)*. Retrieved from https://www.cesm.ucar.edu/community-projects/lens2/data-sets

Conrick, C., & Mass, C. F. (2023). The influence of soil moisture on the historic 2021 Pacific Northwest heatwave. *Monthly Weather Review*, *151*(5), 1213–1228. https://doi.org/10.1175/MWR-D-22-0253.1

Deser, C., Knutti, R., Solomon, S., & Phillips, A. S. (2012). Communication of the role of natural variability in future North American climate. *Nature Climate Change*, *2*(11), 775–779. https://doi.org/10.1038/nclimate1562

Deutsche Welle. (2023). Mexico: Heat Wave Claims Over 100 Lives. Retrieved from https://www.dw.com/en/mexico-heat-wave-claims-over-100-lives/a-66077383

Domeisen, D. I. V., Eltahir, E. A. B., Fischer, E. M., Knutti, R., Perkins-Kirkpatrick, S. E., Schär, C., et al. (2023). Prediction and projection of heatwaves. *Nature Reviews Earth & Environment*, *4*(1), 36–50. https://doi.org/10.1038/s43017-022-00371-z

Douglas, E. (2023). Emergency Room Visits Surge, Texans die Amid Dangerous Heat Wave. Retrieved from https://www.texastribune.org/2023/06/30/texas-heat-wave-deaths-illness/

Englehart, P. J., & Douglas, A. V. (2005). Changing behavior in the diurnal range of surface air temperatures over Mexico. *Geophysical Research Letters*, *32*(1), L01701. https://doi.org/10.1029/2004GL021139

Faranda, D., Bourdin, S., Ginesta, M., Krouma, M., Noyelle, R., Pons, F., et al. (2022). A climate-change attribution retrospective of some impactful weather extremes of 2021. *Weather and Climate Dynamics*, *3*(4), 1311–1340. https://doi.org/10.5194/wcd-3-1311-2022

García-Cueto, O. R., López-Velázquez, J. E., Bojórquez-Morales, G., Santillán-Soto, N., & Flores-Jiménez, D. E. (2020). Trends in temperature extremes in selected growing cities of México under a non-stationary climate. *Atmósfera*, *34*(3), 233–254. https://doi.org/10.20937/atm.52784

Gettelman, A., Hannay, C., Bacmeister, J. T., Neale, R. B., Pendergrass, A. G., Danabasoglu, G., et al. (2019). High climate sensitivity in the Community Earth System Model version 2 (CESM2). *Geophysical Research Letters*, *46*(14), 8329–8337. https://doi.org/10.1029/2019GL083978

Hersbach, H., Bell, B., Berrisford, P., Biavati, G., Horanyi, A., Munoz Sabater, J., et al. (2023). ERA5 hourly data on pressure levels from 1940 to present [Dataset]. *Copernicus Climate Change Service (C3S) Climate Data Store (CDS)*. https://doi.org/10.24381/cds.bd0915c6

Hoerling, M., Kumar, A., Dole, R., Nielsen-Gammon, J. W., Eischeid, J., Perlwitz, J., et al. (2013). Anatomy of an extreme event. *Journal of Climate*, *26*(9), 2811–2832. https://doi.org/10.1175/JCLI-D-12-00270.1

Hong, S. Y., & Kalnay, E. (2000). Role of sea surface temperature and soil-moisture feedback in the 1998 Oklahoma-Texas drought. *Nature*, *408*(6814), 842–844. https://doi.org/10.1038/35048548

Huang, Z., Tan, X., & Liu, B. (2024). Relative contributions of large-scale atmospheric circulation dynamics and anthropogenic warming to the unprecedented 2022 Yangtze River Basin heatwave. *Journal of Geophysical Research: Atmospheres*, *129*(4), e2023JD039330. https://doi.org/10.1029/2023jd039330

Jézéquel, A., Yiou, P., & Radanovics, S. (2018). Role of circulation in European heatwaves using flow analogues. *Climate Dynamics*, *50*(3), 1145–1159. https://doi.org/10.1007/s00382-017-3667-0

Kalashnikov, D. A. (2025a). Supporting datasets for Mexico-Texas heatwave analysis (version 4) [Dataset]. *Zenodo*. https://doi.org/10.5281/zenodo.10901655

Kalashnikov, D. A. (2025b). Code for June 2023 Mexico-Texas heatwave paper (version 2) [Software]. *Zenodo*. https://doi.org/10.5281/zenodo.13845125

Keellings, D., & Moradkhani, H. (2020). Spatiotemporal evolution of heat wave severity and coverage across the United States. *Geophysical Research Letters*, *47*(9), e2020GL087097. https://doi.org/10.1029/2020gl087097

Koster, R. D., Sud, Y. C., Guo, Z., Dirmeyer, P. A., Bonan, G., Oleson, K. W., et al. (2006). GLACE: The global land–atmosphere coupling experiment. Part I: Overview. *Journal of Hydrometeorology*, *7*(4), 590–610. https://doi.org/10.1175/JHM510.1

Lal, P., Singh, G., Das, N. N., Colliander, A., & Entekhabi, D. (2022). Assessment of ERA5-Land volumetric soil water layer product using in situ and SMAP soil moisture observations. *IEEE Geoscience and Remote Sensing Letters*, *19*, 2508305. https://doi.org/10.1109/LGRS.2022.3223985

Lehner, F., & Deser, C. (2023). Origin, importance, and predictive limits of internal climate variability. *Environmental Research: Climate*, *2*(2), 023001. https://doi.org/10.1088/2752-5295/accf30

Lemus-Canovas, M., Insua-Costa, D., Trigo, R. M., & Miralles, D. G. (2024). Record-shattering 2023 Spring heatwave in western Mediterranean amplified by long-term drought. *npj Climate and Atmospheric Science*, *7*(1), 25. https://doi.org/10.1038/s41612-024-00569-6

Li, M., Wu, P., & Ma, Z. (2020). A comprehensive evaluation of soil moisture and soil temperature from third-generation atmospheric and land reanalysis data sets. *International Journal of Climatology*, *40*(13), 5744–5766. https://doi.org/10.1002/joc.6549

Lopez, H., Lee, S.-K., West, R., Kim, D., & Jia, L. (2024). The longest-lasting 2023 western North American heat wave was fueled by the record-warm Atlantic Ocean. *Research Square version 1*. https://doi.org/10.21203/rs.3.rs-5522259/v1

Marvel, K., Su, W., Delgado, R., Aarons, S., Chatterjee, A., Garcia, M. E., et al. (2023). Climate trends. In A. R. Crimmins, C. W. Avery, D. R. Easterling, K. E. Kunkel, B. C. Stewart, & T. K. Maycock (Eds.), *5th National Climate Assessment*. U.S. Global Change Research Program.

McKinnon, K. A., & Simpson, I. R. (2022). How unexpected was the 2021 Pacific Northwest heatwave? *Geophysical Research Letters*, *49*(18), e2022GL100380. https://doi.org/10.1029/2022gl100380

Meehl, G. A., Arblaster, J. M., Bates, S., Richter, J. H., Tebaldi, C., Gettelman, A., et al. (2020). Characteristics of future warmer base states in CESM2. *Earth and Space Science*, *7*(9), e2020EA001296. https://doi.org/10.1029/2020EA001296

Meehl, G. A., Teng, H., Rosenbloom, N., Hu, A., Tebaldi, C., & Walton, G. (2022). How the Great Plains Dust Bowl Drought spread heat extremes around the Northern Hemisphere. *Scientific Reports*, *12*(1), 17380. https://doi.org/10.1038/s41598-022-22262-5

Miralles, D. G., Gentine, P., Seneviratne, S. I., & Teuling, A. J. (2019). Land-atmospheric feedbacks during droughts and heatwaves: State of the science and current challenges. *Annals of the New York Academy of Sciences*, *1436*(1), 19–35. https://doi.org/10.1111/nyas.13912

Miralles, D. G., van den Berg, M. J., Teuling, A. J., & de Jeu, R. A. M. (2012). Soil moisture-temperature coupling: A multiscale observational analysis. *Geophysical Research Letters*, *39*(21), L21707. https://doi.org/10.1029/2012GL053703

Murray-Tortarolo, G. N. (2021). Seven decades of climate change across Mexico. *Atmósfera*, *34*(2), 217–226. https://doi.org/10.20937/atm.52803

National Academies of Sciences, Engineering, and Medicine (NASEM). (2016). *Attribution of Extreme Weather Events in the Context of Climate Change*. National Academies Press.

National Centers for Environmental Information (NCEI). (2024). Climate Monitoring Records. Retrieved from https://www.ncei.noaa.gov/access/monitoring/monthly-report/synoptic/202306

National Weather Service (NWS). (2023). *Climate and Weather Summary for June 2023*. National Weather Service. Retrieved from https://www.weather.gov/media/sjt/pdf/Jun2023Highlights.pdf

Neal, E., Huang, C. S. Y., & Nakamura, N. (2022). The 2021 pacific northwest heat wave and associated blocking: Meteorology and the role of an upstream cyclone as a diabatic source of wave activity. *Geophysical Research Letters*, *49*(8), e2021GL097699. https://doi.org/10.1029/2021gl097699

Otto, F. E. L. (2023). Attribution of extreme events to climate change. *Annual Review of Environment and Resources*, *48*(1), 813–828. https://doi.org/10.1146/annurev-environ-112621-083538

Perkins-Kirkpatrick, S. E., & Lewis, S. C. (2020). Increasing trends in regional heatwaves. *Nature Communications*, *11*(1), 3357. https://doi.org/10.1038/s41467-020-16970-7

Philip, S. Y., Kew, S. F., van Oldenborgh, G. J., Anslow, F. S., Seneviratne, S. I., Vautard, R., et al. (2022). Rapid attribution analysis of the extraordinary heat wave on the Pacific coast of the US and Canada in June 2021. *Earth System Dynamics*, *13*(4), 1689–1713. https://doi.org/10.5194/esd-13-1689-2022

Pskowski, M., & Gina, J. (2023). Emergency room visits and 911 calls for heat illness spike during Texas heat wave. Retrieved from https://insideclimatenews.org/news/28062023/texas-heat-illness-emergency-visits/

Qiao, L., Zuo, Z., Zhang, R., Piao, S., Xiao, D., & Zhang, K. (2023). Soil moisture-atmosphere coupling accelerates global warming. *Nature Communications*, *14*(1), 4908. https://doi.org/10.1038/s41467-023-40641-y

Rodgers, K. B., Lee, S.-S., Rosenbloom, N., Timmermann, A., Danabasoglu, G., Deser, C., et al. (2021). Ubiquity of human-induced changes in climate variability. *Earth System Dynamics*, *12*(4), 1393–1411. https://doi.org/10.5194/esd-12-1393-2021

Rupp, D. E., S. Li, N. M., Sparrow, S. N., Mote, P. W., & Allen, M. (2015). Anthropogenic influence on the changing likelihood of an exceptionally warm summer in Texas, 2011. *Geophysical Research Letters*, *42*(7), 2392–2400. https://doi.org/10.1002/2014GL062683

Seager, R., Goddard, L., Nakamura, J., Henderson, N., & Lee, D. E. (2014). Dynamical causes of the 2010/11 Texas–northern Mexico drought. *Journal of Hydrometeorology*, *15*(1), 39–68. https://doi.org/10.1175/JHM-D-13-024.1

Seneviratne, S. I., Zhang, X., Adnan, M., Badi, W., Dereczynski, C., Di Luca, A., et al. (2021). Weather and climate extreme events in a changing climate. In *Climate Change 2021: The Physical Science Basis. Contribution of Working Group I to the Sixth Assessment Report of the Intergovernmental Panel on Climate Change*. Cambridge University Press.

Singh, D., Bekris, Y. S., Rogers, C. D. W., Doss-Gollin, J., Coffel, E. D., & Kalashnikov, D. A. (2024). Enhanced solar and wind potential during widespread temperature extremes across the U.S. interconnected energy grids. *Environmental Research Letters*, *19*(4), 044018. https://doi.org/10.1088/1748-9326/ad2e72

Stahle, D. W., Cook, E. R., Díaz, J. V., Fye, F. K., Burnette, D. J., Griffin, D., et al. (2009). Early 21st-century drought in Mexico. *Eos*, *90*(11), 89–90. https://doi.org/10.1029/2009EO110001

Stillman, D., Samuel, J., & Voisard, A. (2023). Dangerous extreme heat topples records around the world. *Washington Post*. Retrieved from https://www.washingtonpost.com/weather/interactive/2023/heat-extremes-china-mexico-texas-india/

Swain, D. L., Singh, D., Touma, D., & Diffenbaugh, N. S. (2020). Attributing extreme events to climate change: A new frontier in a warming world. *One Earth*, *2*(6), 522–527. https://doi.org/10.1016/j.oneear.2020.05.011

Terray, L. (2021). A dynamical adjustment perspective on extreme event attribution. *Weather and Climate Dynamics*, *2*(4), 971–989. https://doi.org/10.5194/wcd-2-971-2021

Terray, L. (2023). A storyline approach to the June 2021 northwestern North American heatwave. *Geophysical Research Letters*, *50*(5), e2022GL101640. https://doi.org/10.1029/2022GL101640

Tippett, M. K., & DelSole, T. (2013). Constructed analogs and linear regression. *Monthly Weather Review*, *141*(7), 2519–2525. https://doi.org/10.1175/MWR-D-12-00223.1

Trok, J. T., Barnes, E. A., Davenport, F. V., & Diffenbaugh, N. S. (2024). Machine learning-based extreme event attribution. *Science Advances*, *10*(34), adl3242. https://doi.org/10.1126/sciadv.adl3242

van den Dool, H. M. (1994). Searching for analogues, how long must we wait? *Tellus*, *46*(3), 314–324. https://doi.org/10.1034/j.1600-0870.1994.t01-2-00006.x

van Oldenborgh, G. J., Wehner, M. F., Vautard, R., Otto, F. E. L., Seneviratne, S. I., Stott, P. A., et al. (2022). Attributing and projecting heatwaves is hard: We can do better. *Earth's Future*, *10*(6), e2021EF002271. https://doi.org/10.1029/2021EF002271

Wehrli, K., Guillod, B. P., Hauser, M., Leclair, M., & Seneviratne, S. I. (2019). Identifying key driving processes of major recent heat waves. *Journal of Geophysical Research: Atmospheres*, *124*(22), 11746–11765. https://doi.org/10.1029/2019JD030635

Yiou, P., Jézéquel, A., Naveau, P., Otto, F. E. L., Vautard, R., & Vrac, M. (2017). A statistical framework for conditional extreme event attribution. *Advances in Statistical Climatology Meteorology and Oceanography*, *3*(1), 17–31. https://doi.org/10.5194/ascmo-3-17-2017

Yiou, P., Vautard, R., Naveau, P., & Cassou, C. (2007). Inconsistency between atmospheric dynamics and temperatures during the exceptional 2006/2007 fall/winter and recent warming in Europe. *Geophysical Research Letters*, *34*(21), L21808. https://doi.org/10.1029/2007GL031981

Zhuang, Y., Fu, R., Santer, B. D., Dickinson, R. E., & Hall, A. (2021). Quantifying contributions of natural variability and anthropogenic forcings on increased fire weather risk over the western United States. *Proceedings of the National Academy of Sciences of the United States of America*, *118*(45), e2111875118. https://doi.org/10.1073/pnas.2111875118

Zscheischler, J., & Seneviratne, S. I. (2017). Dependence of drivers affects risks associated with compound events. *Science Advances*, *3*(6), e1700263. https://doi.org/10.1126/sciadv.1700263